3D printed re-entrant cavity resonator for complex permittivity measurement of crude oils

Mohammed, Ali M.; Hart, Abarasi; Wood, Joe; Wang, Yi; Lancaster, Michael J.

DOI:
10.1016/j.sna.2020.112477

3D Printed Re-entrant Cavity Resonator for Complex Permittivity Measurement of Crude oils

Ali M. Mohammed[1*], Abarasi Hart[2], Joe Wood[2], Yi Wang[3] and Michael J. Lancaster[3]

[1]Federal Polytechnic Damaturu, Nigeria and Department of Electronic, Electrical and Systems Engineering, University of Birmingham
[2]School of Chemical Engineering, University of Birmingham
[3]School of Engineering, Department of Electronic, Electrical and Systems Engineering University of Birmingham, United Kingdom

Abstract

This paper presented a microwave resonator-based dielectric metrology technique using a new unified analytical model to extract complex permittivity of low-loss liquid materials. The main design drive of the modified re-entrant cavity is to confine the electric field and therefore enhance the interaction with the material under test while maintaining high quality factor of the cavity. This enables high sensitivity when measuring complex permittivity of low loss materials. The fabrication of the resonator was made easy by using stereo-lithography (SLA) 3D printing. The measured resonance frequency of the fabricated cavity is 2.09 GHz and the quality factor is 5250. The device was first validated using several common solvents. A unified analytical perturbation model based on simulations is developed for the extraction of the complex permittivity. The influence of the dielectric constant on the loss-tangent model has been fully taken into account. Results obtained agree very well with literature values. The device has subsequently been used in the measurement of crude oil samples and the correlation between permittivity measurement and crude oil category has been established.

Keywords*:* permittivity; quality factor; re-entrant cavity; 3D printing; crude oil

*Corresponding author
Email: alimusa02@yahoo.co.uk/amm338@bham.ac.uk

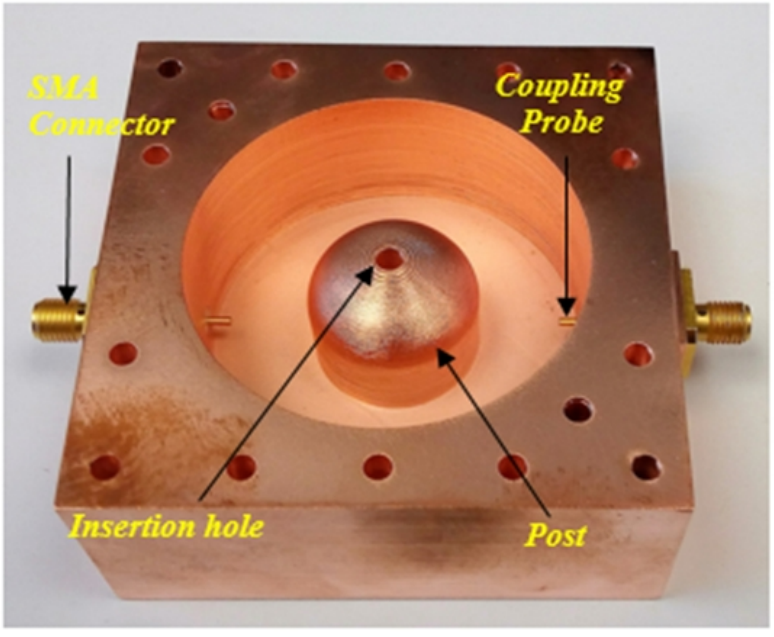

Photo of Prototype Re-entrant Cavity Resonator

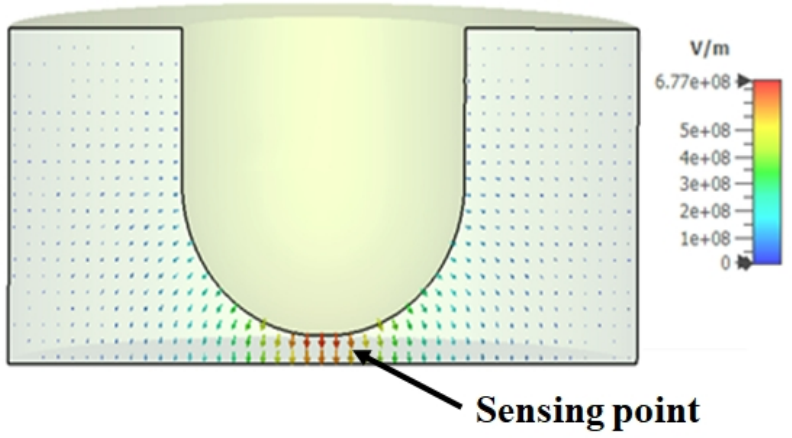

Electric Field Intensity Pattern

Keywords*:* permittivity; quality factor; re-entrant cavity; 3D printing; crude oil

1. Introduction

Microwave re-entrant cavity resonators have been widely studied and used in permittivity measurement. This can be attributed to their high-quality factor and highly confined electromagnetic fields [1]-[7]. Since the introduction of the theoretical analysis by Hansen [1] and further work involving the use of equivalent circuit determined from experimental measurement [2], various geometries of the resonator have been proposed and utilized in material measurements. This includes, for example, a cylindrical single re-entrant cavity for moisture content measurement in solids [3], a tunable re-entrant cavity [4], and an evanescent mode re-entrant cavity with conical post fed by microstrip lines [5]. Others are re-entrant microwave cavity based microfluidic sensors [6] and substrate integrated waveguide re-entrant cavities [7].

There has been an increasing interest in the measurement of dielectric properties of reservoir fluids such as crude oil and their derivatives using microwave sensing techniques [8]-[11]. The focus has largely been on water content measurements, as the high permittivity of water allows for easier determination of its presence in crude oil. This type of measurement relies on a mixing model for reliable estimate of the permittivity values for the emulsion [9]. During the exploration of crude oil at the well site, the crude comes with certain amount of water that needs to be removed. The water content of crude oil in the well is therefore an important factor in determining the oil well recovery rate. On the other hand, the asphaltene fraction is the most polar and heaviest fraction of the crude oil. The polarity of the asphaltene has been linked to its stability [10], which could cause precipitations of the asphaltenes - a detrimental effect on the oil production [11]. Therefore, determining the polarity of asphaltenes in the crude oil is crucial in the production process control [12]. Recently, two multi-point resonant cavities have been used for the analysis of crude oil samples providing a measurement of permittivity from 170 MHz to 8.6 GHz [13]. In [14], an active microwave resonator sensor was used for detection and measurement of asphaltene content in heavy crude oils. The analysis in [14] shows that the real part of the relative permittivity can be related proportionally to the asphaltene content and density of the crude oils. Various studies have shown that an accurate measurement of water content, and analysis of the fractions of saturates, aromatics, resins and asphaltenes (SARA) in crude oil via permittivity measurement would provide a platform for evaluating the performance of oil production and the economic life span of reservoirs [8] – [14]. Traditional methods used for these measurements usually involve chemicals and sophisticated equipment and can be resource intensive. Microwave permittivity measurements are promising for possible utilization in this regard. The technology has the benefit of flexibility because of its wide operational frequency range, its non-invasive nature, and the functionality rendered by its sensitivity and selectivity [15]. For this, a new re-entrant cavity resonator, enabled by additive manufacturing technique, is proposed here.

In conventional re-entrant cavities, as shown in Fig. 1(a), there is a significant trade-off between the field concentration and the quality factor because of the flat base of the centre post. While the electric field increases with a reducing gap *d*, the resistive loss increases too due to excessive concentration of the field around the sharp edges giving a reduced quality factor. In this work a modified re-entrant cavity geometry is proposed as shown in Fig. 1(b). The modification is aimed at confining the electric field at the point where material is place for measurement, while maintaining high cavity quality factor for the sake of sensitivity. The round base avoids the electric field build-up over corners and edges. The field is effectively focused around the tip. Detailed comparison between the flat and curve post will be given in Section 2. Although this is a simple geometry change, the machining of the rounded post is not straightforward for conventional milling. So, an additive manufacturing technique based on stereo-lithography (SLA) 3D printing is used to produce the device.

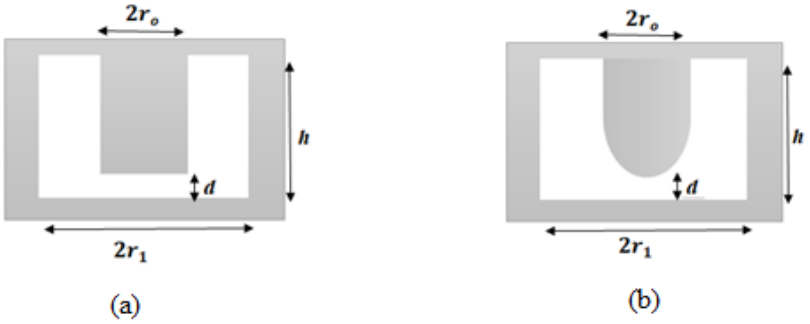

Fig. 1. Re-entrant cavity: (a) Conventional structure (b) Modified structure

2. Eigen mode analysis of re-entrant cavities

The two geometries of Fig. 1 were analyzed and compared using Eigen-mode simulations by Computer Simulation Technology (CST) software [16]. The gap between the top post and cavity adjusts the mode of frequency and traps the electric field within the gap. The dominant TM_{010} mode [17] is utilized in this design.

Table 1. Eigen mode analysis results of the cavities

S/N	Gap, d (mm)	Post profile	Frequency (GHz)	Quality factor	Electric field strength (V/m)	Cavity geometry dimensions		
						h (mm)	r_1 (mm)	r_o (mm)
1	2	Flat	2.072	4432	4.50×10^8	13.35	25.00	11.25
2	2	Curve	2.072	6104	6.75×10^8	24.00	25.00	11.25
3	2	Flat	2.072	4731	5.75×10^8	11.85	25.00	7.50

In the parametric study, the radius (r_0 in Fig. 1) of the post (both flat and curved designs) and that of the cavity (r_1) are kept the same. The height of the cavity is varied to maintain the same gap d for the same resonance frequency as in the cases of row 1 and 2 of Table 1. In the case of row 3 (flat post) both the height and the post radius were adjusted whist keeping the cavity radius r_1 and the gap d for the same resonance frequency. In both cases, the modified (curve post) geometry shows higher magnitude of electric field strength of 6.75×10^8 V/m and higher quality factor (Q-factor) of 6104 in simulation, as compared with the conventional re-entrant cylindrical cavity. Reducing the radius of the flat post or changing gap d may increase the quality factor, but this will lower the electric field strength and therefore the sensitivity. A further study reveals that the curve post geometry gives a higher Q-factor irrespective of the post radius under the same resonance frequency, as shown in Fig. 2. In this parameter study, the height h of the cavity is adjusted while keeping the cavity radius r_1 and the gap d. The highest Q-factor of 5800 is recorded for the flat post at a post radius of 5 mm which is about 5 % less than that of the curved post.

The electric field patterns of the conventional and modified geometry are illustrated in Fig. 3. The high-quality factor and concentration of electric field at the post tip of the modified cavity resonator is highly desired for the increase of device sensitivity [7]. The emphasis on the Q-factor and its relevance in this work is further described in Section 3.

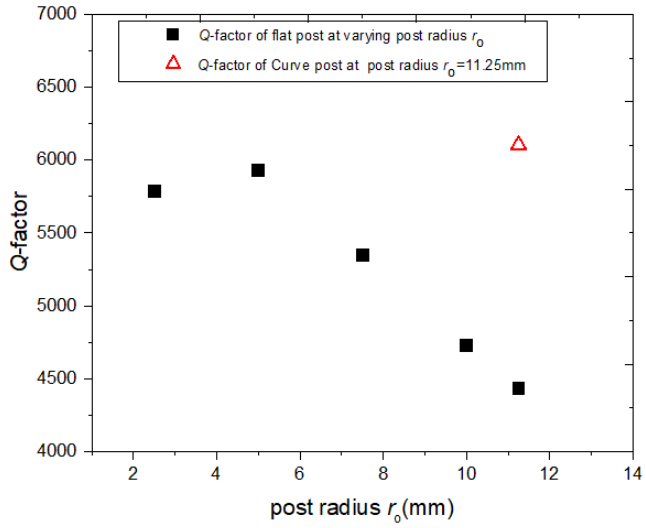

Fig. 2. Simulated quality factor against radius of the post

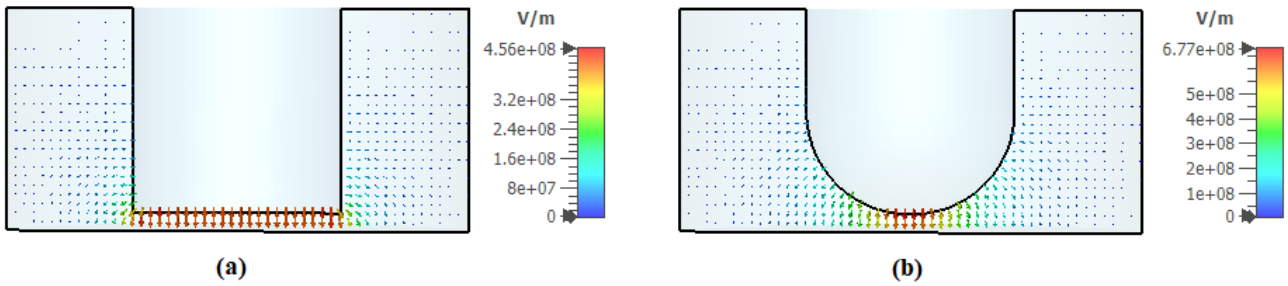

Fig. 3. Electric field patterns: (a) Conventional re-entrant cylindrical cavity (b) Modified (curve post) cavity

3. Sensor design and fabrication

The measurement cavity was designed to operate at a center frequency of 2.0 GHz. It has a radius, $r_1 = 25$ mm and a height, $h = 24$ mm. The post has a radius, $r_0 = 11.25$ mm and the gap, $d = 2$ mm. The base of the post was rounded by a curvature with a radius, $r_b = 11$ mm as shown in Fig. 4. A hole of a diameter of $2r_t = 3.4$ mm was made at the center of the post where a tube is inserted as a sample holder as illustrated in Fig. 4. A transmission-type configuration is adopted for the measurement. The external coupling is via probe of a subminiature A (SMA) coaxial connectors placed on the side walls of the cavity to predominantly couple the electric field of the resonator. The two ports are made identical, and the probes have a diameter of 1.3 mm and a length of 2.9 mm penetrating into the cavity. The probes are positioned toward the joint between the post and the cavity where the electric field intensity is low. This reduces the external coupling level and minimizes the loading effect of the probes.

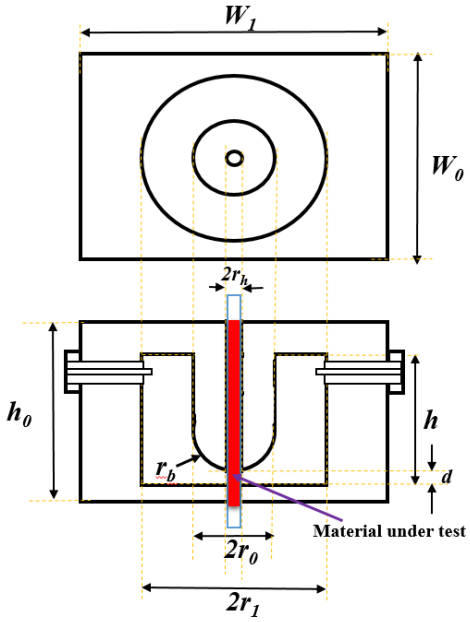

Fig. 4. Top and cross-sectional view of the re-entrant cavity. The dimensions in millimeter are: $W_1 = W_0 = 70$, $h = 24$, $h_0 = 45$, $r_1 = 25$, $r_0 = 11.25$, $r_h = 3.4$ $r_b = 11$, $d = 2$.

These design parameters give a simulated resonance frequency of 2.082 GHz, a loaded quality factor of 5920 and insertion loss of 28.8 dB without the hole. The CST frequency domain solver based on finite element technique (FET) was used with adaptive mesh refinement for the simulation. Following the introduction of the hole into the design, there was a slight increase in frequency to 2.089 GHz and the loaded quality factor had a negligible change as will be discussed further. The insertion loss is 28.6 dB at 2.089 GHz. The material under test fills the entire tube, but only interacts with the E-field in the gap d between the post and the base of the cavity as shown in Fig. 4. The coupling into and out of the cavity is made weak (i.e. large external quality factor Q_e) to achieve the insertion loss of over 20 dB. The loaded Q is defined as [18]

$$Q_l = \frac{f_o}{\Delta f_{3-dB}} \tag{1}$$

where f_o is the resonance frequency and Δf_{3-dB} is the 3-dB bandwidth. The relationships between loaded, unloaded and external Q of the resonator are [18, 19],

$$S_{21}|_{dB} = 20\log\left(Q_l/Q_e\right) \tag{2}$$

$$Q_u = \frac{Q_l}{1 - S_{21}(f_o)} \tag{3}$$

$$\frac{1}{Q_l} = \frac{1}{Q_u} + \frac{1}{Q_e} \tag{4}$$

where Q_l , Q_u and Q_e are the loaded, unloaded and external quality factors respectively. S_{21} is the magnitude of the transmission coefficient. Typically, it is assumed that if $S_{21}(f_o) << 1$ then $Q_u \approx Q_l$, however in this case this is not assumed and (3) is used to extract the unloaded Q. The unloaded Q-factor Q_u is attributed to the conductor loss, radiation loss through

the hole, dielectric loss of the tube and loss due to the sample under test. These are represented by Q_c, Q_r, Q_t and Q_s respectively and relate to Q_u as follows [19].

$$\frac{1}{Q_u} = \frac{1}{Q_c} + \frac{1}{Q_r} + \frac{1}{Q_t} + \frac{1}{Q_s} \tag{5}$$

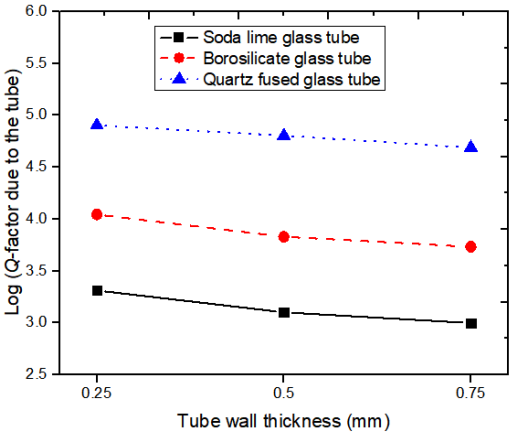

Fig. 5. Q-factor due to the tube with respect to tube wall thickness. The outer diameter is 3 mm in all cases.

The contributions from all these different losses are computed using a series of simulations and (1) to (5) based on the following steps:

1) Starting with a shielded cavity model with copper walls and external energy coupled in and out of the cavity but with no tube hole giving no radiation or dielectric loss. The loaded Q, based on (1) and the magnitude of S_{21}, in dB, can be read from the simulation results. Using (2), the external Q of the resonator, which includes the input and output loading effects, can be estimated.
2) Now that Q_l and Q_e are known, the unloaded Q can be calculated using (3) or (4). Since the only source of internal loss is from the copper conductor in this simulation model, $Q_u = Q_c$ can be deduced from (5).
3) A hole is then introduced into the cavity model. An open boundary simulation gives a new loaded Q-factor. Since the difference between this Q_l and the one from Step 1) is solely a result of the hole and the associated radiation, the radiation loss Q_r is deduced using (3) and (5) as Q_c is known.
4) Now, a tube is inserted into the cavity hole. From the change of the unloaded Q as a result, Q due to the tube Q_t can be extracted.
5) This cavity model, with copper walls, a hole and a tube, under open boundary condition, is used as the reference model to represent the experimental configuration before inserting samples.

Table 2. Nominal dielectric properties of the three glass tubes [20]

Tube	Dielectric constant ε_r'	Loss tangent $tan\delta$
Quartz glass tube	3.75	0.0004
Borosilicate glass Tube	4.30	0.0047
Soda Lime glass tube	6.00	0.0200

Table 3. Values of quality factors contribution based on simulation

Simulated Q-factors	**Q-factor values**
Q-factor due to conductor Q_c	6126
External Q-factor Q_e	1.63×10^5
Q-factor due to radiation Q_r	2.03×10^6
Q-factor due to Quartz glass tube Q_{tq}	43776
Q-factor due to Borosilicate glass tube Q_{tb}	3420
Q-factor due to Soda Lime glass tube Q_{ts}	600

The tubes that are used to hold samples could also have an important impact on the Q-factor. Three types of tubes were considered - borosilicate, quartz fused and soda lime glass tubes. The choice of glass tubes is for easy cleaning and its re-usability irrespective of the type of material passing through it. The rigidity of glass tubes would also help with the placement of the sample and the repeatability of the measurement as compared to polymer tubes. A parametric study using simulation is carried out on each of the tubes with varying wall thickness. The dielectric properties of the tubes used in the simulation are given in Table 2 [20]. The change of Q-factor as a function of wall thickness is shown in Fig. 5. The quartz

tube has much higher Q than the other two types. As also expected, the Q decreases with increasing wall thickness. The Q-factors corresponding to the tubes of 3 mm outer diameter (O.D) and 1.5 mm internal diameter (I.D) are given in Table 3 for comparison with all the other Q-factors computed. As given in Table 3, both Q_e, and Q_r are significantly larger than Q_c and therefore have negligible loading and radiation effect on the cavity. The practical choice of the tube will be discussed in the next section.

The device was fabricated using stereo-lithography (SLA) 3D printing technology. The additive manufacturing process allows the accurate fabrication of the irregular shapes and surfaces quickly and easily. The device was made from Accura 25+ polymer and coated with 25 µm copper. The photo prototype is shown in Fig. 6. The cavity is framed in a block of rectangular shape with a wall thickness of 10 mm. A separate base plate was bolted to the main cavity. Considering the surface current concentrates at the point where the post joins the cavity, the split was made on the base away from the post so that the current disturbance was kept to a minimum. The parts were assembled via fourteen 3 mm × 50 mm threaded rods to ensure good contact.

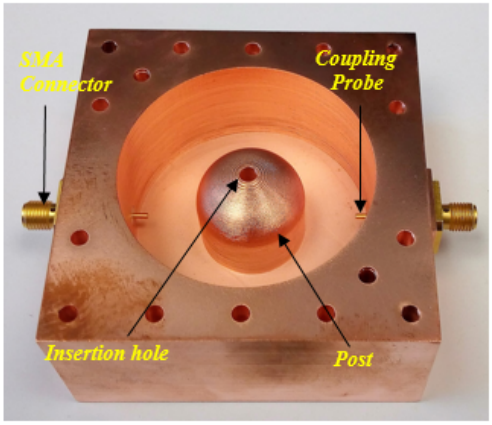

Fig. 6. Photographs of the 3D printed prototype. The flat cover is removed to facilitate viewing.

4. Measurement set up

Measurements were carried out using a PNA network analyzer (Agilent Technology E8382C) which was calibrated with 85052D kit. The measured resonance frequency of the empty cavity with the hole, but no glass tube is 2.094 GHz, with a loaded quality factor of 5250 and insertion loss of 29.3 dB. The measured conductor Q neglecting radiation loss is 5436. As shown in Fig. 7, the measurement and simulation agree very well with a small frequency shift of 5 MHz (0.28 %) and difference in Q-factor of 670 (11.3 %). This is probably due to the fabrication tolerance of around 10 µm and non-perfect cavity assembly as well as non-perfect copper. The uncertainty analysis of all possible factors of errors will be presented in the next section.

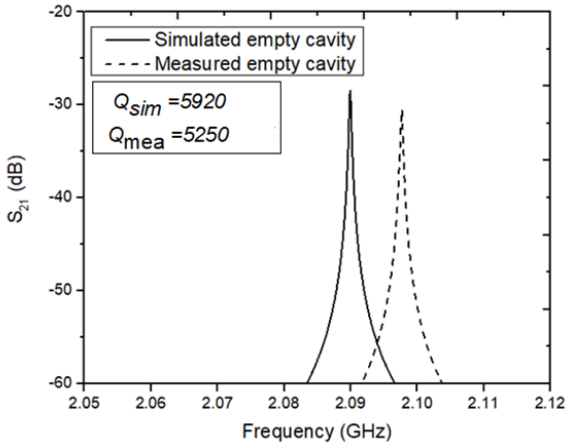

Fig. 7. Measured and simulated S_{21} response of the empty cavity.The simulated and measured loaded Q-factor of the cavity are denoted by Q_{sim} and Q_{mea} respectively

Table 4. Dimensions and associated Q of the three measured glass tubes

Tube	Outer diameter (mm)	Inner diameter (mm)	Wall thickness (mm)	Associated Q from measurement
Quartz glass	3.00	1.50	0.75	126867

Borosilicate glass	3.00	2.98	0.01	52618
Soda Lime glass	1.80	1.24	0.28	3355

Three commercially available tubes have been experimentally examined for their contribution to the *Q*-factor. Their dimensions are given in Table 4. The measured *Q*-factors before and after the tube has been inserted into the hole of the cavity resonator is used in computing the *Q*-value associated with the dielectric loss of the tube. These are also given in Table 4. Both the quartz tube and the thin-wall borosilicate tube exhibit higher *Q*-value than the conductor *Q*, and would have little effect on the overall *Q* of the resonator. However, the thin-wall tube has been found to be too fragile to handle and have large inaccuracy in its dimensions. To this end, the quartz fused tube with 3 mm O.D and 1.5 mm I.D was chosen for this work.

To test the performance of the sensor, three common solvents, Ethanol (99% purity), Acetone (95% and 99% purity), and Methanol (99% purity) from Sigma Aldrich Company Ltd. were measured and analyzed as reference liquids. The liquid samples are passed to the quartz glass tube via a silicone tube with a pipette as shown in the measurement set-up in Fig. 8. The silicone tube is connected at both the inlet and outlet of the quartz tube. As the liquid begins to flow out, the outlet of the silicone tube is sealed. This is to allow static measurement of the liquids and avoid the effect of flow rate. The tube was washed with Isopropanol solvent and dried by gentle heating for 5 minutes before taking any new measurement. New pipettes and silicone tubes are used for each measurement while making sure there were no air bubbles visible as the liquids flows through the transparent tube. The measured S_{21} responses of the cavity, the cavity with the tube and the common solvents are shown in Fig. 9. The changes in quality factors signifies how lossy the samples are, as demonstrated by the respective *Q*-factor due to samples given in Fig 9. The results obtained will be discussed in Section 5.

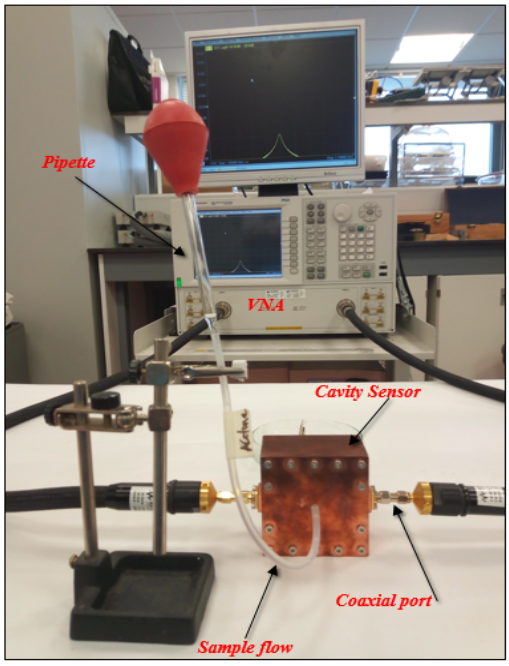

Fig. 8. Photograph of the measurement set-up

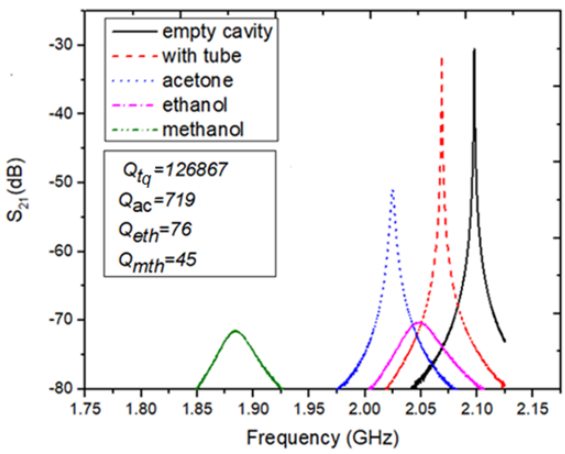

Fig. 9. Measured S_{21} response of the empty cavity, cavity with the tube and with common solvent. The measured Q-factors due to the quartz tube and samples of acetone, ethanol and methanol are denoted by Q_{tq}, Q_{ac}, Q_{eth}, and Q_{mth} respectively.

5. Extraction of complex permittivity

5.1 Simulation based cavity perturbation model

The perturbation method is commonly used for the extraction of complex permittivity of dielectric samples in cavities. The method is considered to work well for measurement of low-loss or medium-loss materials [21]. The changes in resonance frequency and quality factor (Δf and $\Delta(1/Q)$) due to material insertion are utilized in quantifying the complex permittivity of the sample being measured. A cavity perturbation model can be used for a cavity resonator measuring the complex permittivity $\varepsilon_r = \varepsilon_r^{'} - j\varepsilon_r^{''}$ as [22].

$$\varepsilon_r^{'} = A^{-1}\frac{V_c}{V_s}\left(\frac{f_o - f_1}{f_o}\right) + 1 \tag{6}$$

$$\varepsilon_r^{''} = B^{-1}\frac{V_c}{V_s}\left(\frac{1}{Q_0} - \frac{1}{Q_1}\right) \tag{7}$$

where $\varepsilon_r^{'}$ and $\varepsilon_r^{''}$ are the real and imaginary part of the complex permittivity. V_s, is the sample volume exposed to E-field, and V_c is the volume of the cavity. The coefficient A and B are determined by the shape, size, and location of the sample as well as the mode of excitation. The resonance frequency and quality factor of the cavity before and after insertion of the sample are f_o, Q_o and f_1, Q_1 respectively. The coefficients in (6) and (7) can be mathematically determined only for cavity structures with high symmetry and analytically solvable fields [21]. However, this is not the case for the cavity used in this work. Therefore, we have developed a model based on simulations as discussed below. The change in resonance frequency with varying $\varepsilon_r^{'}$ over the range from 1 to 80 at a fixed loss tangent, tanδ, is established by simulation and plotted in Fig. 10. This is used to model the real part of the permittivity. It should be noted, that increasing the loss tangent up to a value of 0.1 has negligible effect on the relationship between $\varepsilon_r^{'}$ and $\Delta f/f_c$ as can be seen from Fig. 10 where three curves are overlapping each other. A quadratic curve fitting gives the following relationship for the extracted real part of the complex permittivity;

$$\varepsilon_r^{'} = 12257.96\left(\frac{\Delta f}{f_c}\right)^2 + 762.1\frac{\Delta f}{f_c} + 1.05 \tag{8}$$

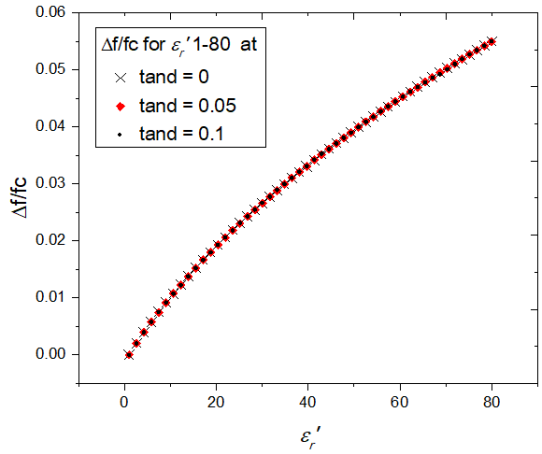

Fig. 10. Relationship between change in resonance frequency and permittivity $\varepsilon_r^{'}$. The three sets of data corresponding to three different tanδ values overlap onto each other.

The model for the imaginary part (i.e. the dielectric loss) is more complicated as the change of the dielectric constant as well as the loss tangent will have an impact on the cavity quality factor. This is because the change of the dielectric constant alters the field. Therefore, a fixed perturbation model will not apply to different materials with significantly different dielectric constants [7]. To deal with this, we first obtained results by simulating the change in $1/Q$ due of the sample as a function of a varying tanδ from 0.001 to 0.2 for a number of $\varepsilon_r^{'}$ values. As shown in Fig. 11, a linear relationship was observed. However, as $\varepsilon_r^{'}$ increases the slope increases. From the data obtained we can derive,

$$\Delta(1/Q) = P(\varepsilon_r^{'}) \cdot \tan(\delta) + M \tag{9}$$

where P is a function of ε_r' and M is treated as a constant close to zero. The dependence of P on $\varepsilon_r^{'}$ is then investigated at a fixed tanδ. The simulated relationship between $\varepsilon_r^{'}$ and $\Delta(1/Q)$ for a fixed $\tan\delta = 0.2$ is plotted in Fig. 12.

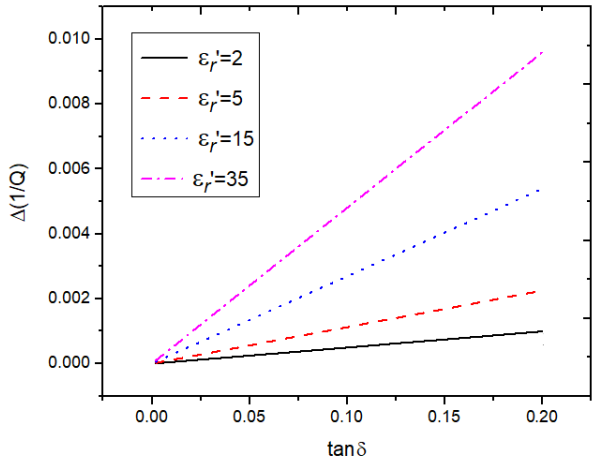

Fig 11. Relationship between the change in quality factor of the material under test and loss tangent at different permittivity values

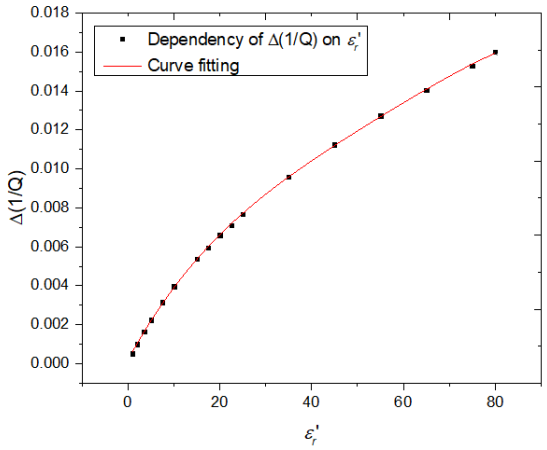

Fig 12. Relationship between changes in quality factor as a function of permittivity when tan (δ) = 0.2.

A polynomial fitting of Fig. 12 gives

$$\Delta(1/Q)|_{tan(\delta)\,=\,0.2} = A_1\varepsilon_r^{'4} + A_2\varepsilon_r^{'3} + A_3\varepsilon_r^{'2} + A_4\varepsilon_r^{'} + C \tag{10}$$

where

$$\begin{cases} A_1 = -3.75 \times 10^{-10} & A_2 = 8.3 \times 10^{-8} \\ A_3 = -7.23 \times 10^{-6} & A_4 = 4.36 \times 10^{-4} \\ & C = 1.82 \times 10^{-4} \end{cases}$$

The function $P(\varepsilon_r^{'})$ can then be deduced from

$$P(\varepsilon_r^{'}) = \frac{\Delta(1/Q)|_{tan(\delta)\,=\,0.2} - M}{0.2} \tag{11}$$

Substituting (9) into (7) we can arrive at a unified relationship for determining the loss tangent as;

$$tan\delta = \frac{0.2\left(\Delta\left(\frac{1}{Q}\right) - \mathrm{M}\right)}{\Delta(1/Q)|_{tan(\delta)\,=\,0.2} - \mathrm{M}} \tag{12}$$

where the constant $M = 3.27 \times 10^{-7}$ can be taken as negligible. The imaginary part can be calculated based on the results obtained in (8) and (12) using the equation;

$$\varepsilon_r^{''} = \varepsilon_r^{'} \times tan\delta \tag{13}$$

The coefficient of determination also known as R-squared [23], a measure of the accuracy of the curve fitting, is 0.9999 in all the curve fittings of the mathematical models above indicating good fit of the equations (8) and (10) with the simulated results. On the other hand, due to fabrication tolerance the designed cavity cannot be accurately made to its exact dimensions. So there would be some difference between the design cavity in CST and the fabricated device. However, based on the very small difference between the measured and simulated results as presented in Section 4, additional calibration of the model is not required in this case. The curve fitted extraction model is based on the difference between two values (before and after sample insertion) rather than the absolute values. Therefore, the discrepancy (very small in this case) between the absolute measurement and simulation will be largely cancelled out. However, any residual error due to this factor is included in the error analysis as would be describe in the next Section.

5.2 Error analysis and uncertainty evaluation

In the relative permittivity and loss tangent measurement using the designed cavity sensor, there are a number of sources for errors. These include dimensional errors of the tube, the hole and the cavity, system errors in the model described in section 5.1 and measurement uncertainties due to temperature instability, random errors from the S-parameter measurements (including calculation of the Q values). There is also measurements repeatability of the device and the set-up. These errors combine together and an estimation of their effect is discussed below.

The uncertainties resulting from the abovementioned factors were determined separately in relation to changes in frequency (for dielectric constants) and quality factor (for loss tangents) based on simulations and measurements. The procedure given in [24] is adopted to compute for individual uncertainty as well as the expanded standard uncertainty and results presented in Table 5. The errors are:

5.2.1 Dimension errors:

CST simulations is utilized to arrive at the uncertainty influenced by the potential dimensional errors. The nominal tolerances of the tube, hole, and cavity, given by the manufacturer (Table 5), were used to obtain separately the potential change in frequency and quality factor resulting from the variations in dimensions. The individual standard uncertainty is then computed.

5.2.2 Temperature variation:

The effect of temperature change was determined based on measurements taken at different temperatures within a variation of ± 1.0 °C from three data sets (n = 3). The standard uncertainty in frequency and quality factor resulting from the changes in temperature were determined accordingly.

5.2.3 Measurements error:

The measurement repeatability was evaluated using methanol as the reference sample by taking five repeated readings and the standard uncertainty for both change in frequency and Q-factor were evaluated.

5.2.4 Extraction model:

The model developed for the extraction of the dielectric properties based on curve fitting of simulations data has some discrepancy between the data and estimation model. The measure of this is the residual sum of square. The change in frequency is related to (8) and Q-factor is associated with (12). This source of error is considered and included in Table 5.

The combined uncertainty in dielectric constant and the loss tangent were evaluated and the expanded uncertainty assuming a normal probability distribution using a coverage factor value k = 2 was computed accordingly [24]. This signifies a confidence level of approximately 95 % [24]. The expanded uncertainty on the dielectric constant is considered, while that of the loss tangents is considered negligible and not included in the results of the measurements (Table 6 and 8).

In order to minimize some of these errors, certain measures were taken as described below. A tube with measured (using micrometer screw gauge) outer diameter of 3.020 mm is used as sample holder. As the dimensions of the tube may vary along the length of the tube, measurements were only taken while maintaining its position relative to the cavity. However, the inner diameter was not measured. To minimize the measurement error, a large number of sweep points (6401), over a bandwidth about five times the 3 dB bandwidth, were used. An IF bandwidth of 50 Hz for high loss materials and 500 Hz for low loss materials is used to reduce effect of noise in the response. All samples were measured four times and the

average was used in computing the dielectric properties. All measurements were carried out within an ambient temperature of 21.0 ± 1.0 °C.

Table 5. Uncertainty analysis based on simulation and measurements

Sources of Uncertainty		**Temp.**	**Cavity dimensions (fabrication tolerances)**	**Outer Diameter of the tube dimension**	**Inner Diameter of the tube dimension**	**Hole dimension**	**Residual sum square of developed model**	**Measurement repeatability**	**Combined**
Tolerance		±1°C	±0.01mm	±0.02mm	±0.02mm	±0.05mm	-	-	-
Uncertainty of resonance frequency and quality factor	$\Delta f/f$	6.17×10^{-3}	2.95×10^{-3}	4.90×10^{-3}	2.20×10^{-3}	2.72×10^{-4}	8.56×10^{-6}	1.82×10^{-4}	8.70×10^{-3}
	$\Delta(1/Q)$	7.45×10^{-7}	5.79×10^{-6} .	8.01×10^{-6}	5.10×10^{-5}	1.78×10^{-6}	9.72×10^{-6}	1.55×10^{-3}	1.55×10^{-3}
Covering factor (k=2)	**Expanded uncertainty on ε_r' is 1.74×10^{-2}**						**Expanded uncertainty on $tan\,\delta$ is 3.10×10^{-3}**		

5.3 Model verification

The real parts of the complex permittivity were extracted using (8) for the three common solvents and the imaginary parts were obtained using (12) and (13). The measured and reported complex permittivity of the common solvents are compared in Table 6. There is a close agreement between the results especially for methanol with the lowest difference of 1.5% with the literature results. Acetone and ethanol recorded a slightly higher difference of 5.2% and 3.9% respectively. It should be noted the small difference could potentially be because the liquids have slightly different purity. The measured results between the two acetone samples with different purity suggest how sensitive the device is to minor changes of concentration or purity. Generally, Table 6 shows our method has produced good agreement with those reported in the literature. This has validated the model developed for the extraction of complex permittivity.

Table 6. Comparison between measured and literature values of permittivity of common solvent at s-band

Samples	Measured	Literature	% Difference in Magnitude between measured and literature
Acetone (99.9% purity)	22.09 ± 0.38 – j0.84	21.40 – j1.02 [25]	3.2
Acetone (95.5% purity)	22.52 ± 0.38 – j0.97	-	5.2
Ethanol (95.5% purity)	8.58 ± 0.15 – j7.42	8.26 – j7.91 [26]	3.9
Methanol (99.9% purity)	25.22 ± 0.44 – j10.8	24.84 – j12.28 [26]	1.5

5.4 Measurement of crude oil

Further measurement of three different samples (S1, S2 & S3) of crude oil as classified by the parameter American Petroleum Institute (API) gravity were carried out [27]. The crude oil samples were chemically characterized in terms of density, viscosity and weight percentage of asphaltenes before the microwave measurements.

An Anton Paar DMA 35 digital density meter was used to measure the specific gravities of the oils, from which the API gravity was calculated. The viscosity was measured using Bohlin Instruments CVO 50 NF rheometer (Malvern Instruments Ltd., UK) at 25 ºC using a shear rate of 100 s^{-1} and a steel parallel plate with 100 µm gap. The asphaltene in the oils was precipitated in accordance with ASTM D2007 [28], by mixing 40 mL n-heptane solvent and 1 g of crude oil sample. The mixture was stirred for about 4 hours using magnetic stirrer and allowed to settle for 24 hours. The asphaltene was then filtered as solid from the oil/precipitant mixture using a standard funnel filter system. The filter paper with the content (asphaltenes) was dried and then weighted. As shown in Table 7, the samples are in the categories of light, medium and heavy crude oil based on their API gravity values. About 15 wt% of asphaltenes was obtained for the heavy oil while only 1 wt% and 2 wt% were obtained for the light and medium crude oils respectively. The deasphalted liquid was then separated from the n-heptane by evaporation at 30 ºC. The dielectric constant and the loss factor of the crude oil, deasphalted oil, and asphaltenes (for heavy oil only) were measured and are presented in Table 8. The properties of asphaltenes for the light and medium oil could not be determined due to low quantities of collected asphaltenes. For the microwave measurement the samples were passed through the tube using the set-up explained earlier except in the case of asphaltenes which is in solid form. For this, the asphaltenes were ground and put into the tube. Compression was applied and sample was measured

and re-measured after further compression to reduce effect of air gap. The measured packing density of the crushed asphaltenes is in the range of 0.5 – 0.6 g/cm^3. However, complete removal of air cannot be ascertained.

Table 7. Properties of the three crude oil samples

Crude Sample	Sample weight (g)	API Gravity (°)	Viscosity @ 25°C (mPa-s)	Asphaltene (wt%)	Specific gravity
S1: Light Crude	2.00	40.58	2.30	1.00	0.8223
S2: Medium Crude	2.00	27.35	9.38	2..00	0.8908
S3: Heavy Crude	28.00	12.80	1483	14. 60	0.9806

Table 8. Comparison between measured and literature values of permittivity of crude oil samples

Samples and crude oil categories		**Dielectric constant $\varepsilon_r^{'}$**			**Loss factor $\varepsilon_r^{''}$**			**Literature values of crude oil** [13] [29]	
		crude oil	**Asphaltenes**	**Deasphalted Oil**	**crude oil**	**Asphaltenes**	**Deasphalted Oil**	**Dielectric constant $\varepsilon_r^{'}$**	**Loss factor $\varepsilon_r^{''}$**
S1	Light oil	2.062 ± 0.038	-	2.370 ± 0.041	0.0141	-	0.010	2.16	0.021
S2	Medium oil	2.254 ± 0.039	-	2.448 ± 0.042	0.0148	-	0.016	2.31	0.020
S3	Heavy oil	2.720 ± 0.047	2.255 ± 0.039	2.524 ± 0.044	0.0159	0.0028	0.018	2.47	0.015

The results of dielectric constants of the original crude oils shows a clear distinction between the three classifications. The dielectric constant increased as the density of the crude oil increased from light to heavy oil (Tables 7 and 8). The trend is similar for the loss factor and was also observed in [13]. The loss factor of the crude oil and the deasphalted are very similar, suggesting less effect of asphaltenes on the loss factor, as also reported by [29]. However, this is contrary to an earlier suggestion [30] that asphaltenes made a significant contribution toward the loss factor of heavy oils. The dielectric constant of the crude oil is higher than that of the asphaltenes in the heavy oil, which agrees well with earlier reported values [12]. This is also in agreement with results obtained for dielectric constant of asphaltenes extracted from vacuum distilled residue (VDR) heavy oil [29, 31]. It has to be said that the results are not conclusive as the extracted asphaltene sample in our study may not have the full density. The deasphalted oil has not been further separated in this work to obtain the fractions of saturates, aromatics and resins. The difference in asphaltenes dielectric properties with the earlier reported data can also be attributed to composition of the crude oil which changes according to source, maturity, thermal chemical sulfate reduction and biodegradation [13].

6. Conclusion

A modified re-entrant cavity resonator has been realized for complex permittivity measurement of liquids sample at 2.0 GHz. A unified analytical formula was developed based on simulation to accurately extract the complex permittivity of the samples. The influence of the dielectric constant on the loss-tangent model has been fully taken into account. The cavity has the advantage of high-quality factor and confined electric field. Experimental tests have been carried out to demonstrate the sensing capabilities of the sensor using several common solvents. Results obtained verified the device capability in permittivity measurement and its sensitivity in purity measurement as seen in the case of acetone. The device has also been used to measure the dielectric properties of three different crude oils as classified by API gravity - light, medium and heavy oils. The correlation between dielectric permittivity and the crude category has been established. The results obtained from the measured dielectric properties reveals that the presence of asphaltenes has less effect on the dielectric loss of the crude oil than other components. A lower dielectric constant than the original oil was obtained in the case of asphaltenes as against earlier reported findings using technique other than cavity perturbation. However, this investigation and comparison is not conclusive due to potential influence from the sample density. This study has now opened up the need to investigate further the asphaltenes properties in relation to crude oil density and viscosity using microwave sensing techniques.

Acknowledgements

This work was supported by Petroleum Development Technology Fund (PTDF), Nigeria by providing scholarship for A.M. Mohammed. The author A. M. Mohammed would also like to thank and appreciate Dr. Stephen Hanham for useful discussion.

References

[1] W. W. Hansen, On the Resonant Frequency of Closed Concentric Lines, J. Appl. Phys., vol. 10, no. 38, pp. 38-45, 1939.

[2] K. Fujisawa, General Treatment of Klystron Resonant Cavities, IRE Trans. Microw. Theory Techn., pp. 344 - 58, 1958.

[3] F. Thompson, A. D. Haigh, B. M. Dillon and ,. A. P. Gibson, Analysis and design of a re-entrant microwave cavity for the characterisation of single wheat grain kernels, IEE Proc. Sci. Meas. Techn., vol. 150, no. 3, pp. 113-117, 2003.

[4] J.-M. Floch, L. Y. Fan, D. M. Aubourg, N. Cros, Q. Carvalho, J. Shan, E. Bourhill and G. Humbert, "Rigorous analysis of highly tunable cylindrical Transverse Magnetic mode reentrant cavities," Rev. Sci. Instrum., vol. 84, pp. 1-7, 2013.

[5] A. Murugkar, R. Panigrahi and K. J. Vinoy, A novel approach for high Q microwave re-entrant cavity resonator at S-band, in Asia-Pacific Microw. Conf (APMC),, New Delhi, 2016.

[6] H. Hamzah, A. Abduljabar, J. Lees and A. Porch, Compact Microwave Microfluidic Sensor Using a Re-Entrant Cavity, Sensors, vol. 18, no. 3, pp. 1-12, 2018.

[7] Z. Wei, J. Huang, J. Li, G. Xu, Z. Ju, X. Liu and X. Ni, A High-Sensitivity Microfluidic Sensor Based on a Substrate Integrated Waveguide Re-Entrant Cavity for Complex Permittivity Measurement of Liquids, Sensors, pp. 1-17, 2018.

[8] A. Porch, D. Slocombe, J. Beutler, P. Edwards, A. Aldawsari, T. Xiao, V. Kuznetsov, H. Almegren, A. Saud and N. Almaqati, Microwave Treatment In Oil Refining, Appl Petrochem Res, vol. 2, no. 1-2, pp. 37-44, 2012.

[9] P. Sharma, L. Lao and G. Falcone, A Microwave Cavity Resonator Sensor for Water-in-oil Measurements, Sensors and Actuators B: Chemical , vol. 262, pp. 200- 210, 2018.

[10] G. Wulfsberg, Inorganic Chemistry, Sausalito, CA: University Science Book, 2000.

[11] H. Belhaj, H. A. Khalifeh and N. Al-Huraibi, Asphaltene Stability in Crude Oil during Production Process, Journal of Petroleum & Environmental Biotechnology, vol. 4, no. 3, pp. 1-5, 2013.

[12] A. Punase and B. Hascakir, Stability Determination of Asphaltenes through Dielectric Constant Measurements of Polar Oil Fractions, Energy Fuels, vol. 31, no. 1, pp. 65-72, 2017.

[13] J. O. Alvarez, ,. D. Jacobi and G. Bernero, Dielectric Characterization of Geochemical Properties of Crude Oils and Gas Condensate at 25ºC, in Geosci. Rem Sens Symp (IGARSS), Fort Worth, 2018.

[14] M. Abdolrazzaghi, M. H. Zarifi, C. F. A. Floquet and M. Daneshmand, Contactless Asphaltene Detection Using an Active Planar Microwave Resonator Sensor, Energy Fuel, vol. 31, no. 8, pp. 8784 - 8791, 2017.

[15] Ali A. Abduljabar David J. Rowe, A. Porch and D. A. Barrow, Novel Microwave Microfluidic Sensor Using a Microstrip Split-Ring Resonator, IEEE Trans. Microw. Theory Techn, vol. 62, no. 3, pp. 679 - 688, 2014.

[16] Computer Simulated Technology, Microwave Studio, 2018. [Online]. Available: http//www.cst.com/.

[17] B. T. McAllister, Y. Shen, G. R. Flower, S. R. Parker and M. E. . Tobar, Higher Order Reentrant Post Modes in Cylindrical Cavities, J. Apply. Phys, vol. 112, pp. 1-8, 2017.

[18] J. Papapolymerou, J.-C. Cheng, J. East and L. Katehi, A micromachined high-Q X-band resonator, IEEE Microw and Guided Wave Lett, vol. 7, no. 6, pp. 168 - 170, 1997.

[19] M. J. Lancaster, Superconductive cavity resonators, in Passive Microwave Device Applictaions Of High Temperature Supercoductors, Cambridge, Cambridge University Press, 1997, pp. 67-125.

[20] K. Fenske and D. Misra, Dielectric Materials At Microwave Frequencies, Applied Microwave & Wireless, vol. 12, no. 10, pp. 92 - 100, 2000.

[21] L. F. Cheng, C. K. Ong, C. P. Neo, V. V. Varandan and V. K. Varadan, Microwave Electronics: Measurement and Materials Characterisation, USA: John Wiley & Sons Ltd, 2004, pp. 251 -270.

[22] L. F. Cheng, C. K. Ong, C. P. Neo, V. V. Varandan and V. K. Varadan, Resonant-perturbation Methods, in Microwave Electronics: Measurement and Materials Characterisation , USA, John Wiley & Sons Ltd, 2004, pp. 251 -270.

[23] E. Kasuya, On The Use Of R And R-Squared In Correlation And Regression, Ecol. Res, vol. 34, p. 235–236., 2019.

[24] S. Bell, A Beginner's Guide to Uncertainty of Measurement, National Physics Laboratory , Middlesex, United Kingdom, 2001.

[25] M. Mohsen-Nia, H. Amiri and B. J. Jazi, Dielectric Constants of Water, Methanol, Ethanol, Butanol and Acetone: Measurement and Computational Study, J. Sol. Chem, vol. 39, p. 701–708, 2010.

[26] A. P. Gregory and R. N. Clarke, Tables of The Complex Permittivity of Dielectric Reference Liquids at Frequencies up to 5 Ghz, National Physical Laboratory, London, 2012.

[27] J. M. Santos, A. Vetere, A. J. Wisniewski, M. N. Eberlin and W. Schrader, Comparing Crude Oils with Different API Gravities on a Molecular Level Using Mass Spectrometric Analysis. Part 2: Resins and Asphaltenes, Energies , vol. 11, no. 2767, pp. 1-14, 2018.

[28] ASTM International. ASTM D2007, Standard Test Method for Characteristic Groups in Rubber Extender and Processing Oils and Other Petroleum-Derived Oils by the Clay-Gel Absorption Chromatographic Method, West Conshohocken, PA: ASTM International, 2007.

[29] Y. Zhang, M. Adam, A. Hart, J. Wood and S. P. Rigby, Impact of Oil Composition on Microwave Heating Behavior of Heavy Oils, Energy Fuel , vol. 32, no. 2, pp. 1592-1599, 2018.

[30] L. Hu, H. A. Li, T. Babadagli and M. Ahmadloo, Experimental investigation of combined electromagnetic heating and solvent-assisted gravity drainage for heavy oil recovery, J. Pet Sci and Eng, vol. 154, pp. 589-601, 2017.

[31] M. Adam, Private Communication, Aug. 2019.

A. M. Mohammed

Ali Musa Mohammed obtained National Diploma and Bachelor of Engineering B-Eng in Electrical and Electronic Engineering from Ramat Polytechnic Maiduguri and University of Maiduguri in 2001 and 2009 respectively. He secured a full scholarship funding with National Information and Technology Development Agency (NITDA) Nigeria, for MSc Wireless Communications Systems Engineering in 2014 with University of Greenwich, UK. He graduated with Distinction and was awarded the Engineering Prize Award for Best overall performance in his MSc Programme cohort by University of Greenwich in 2015. He has been in the academia teaching engineering courses related to his field since July 2011 with Federal Polytechnic Damaturu, Nigeria. He is currently undergoing his PhD research (funded by Petroleum Development Technology Fund, PTDF Nigeria) with Emerging Device Technology (EDT) Research Group of University of Birmingham, United Kingdom. His research is focussed on Microwave Sensing Techniques for material Characterisation and Identification.

He is a member of IEEE and Nigerian Society of Engineers NSE. He has also been awarded the research poster conference people's choice award in 2019 by University graduate school, University of Birmingham.

Abarasi Hart

Abarasi Hart graduated with a BEng in Chemical and Petrochemical Engineering from Niger Delta University in 2006, where he was awarded the Vice Chancellor's medal for best graduating student. He qualified with MSc in Advanced Chemical Engineering from University of Birmingham, UK in 2010, on the award of Joint University of Birmingham and Allan Nesta Ferguson Charitable Scholarship. He obtained his PhD in the same institution with thesis topic advanced studies of catalytic upgrading of heavy oils under the supervision of Prof. Joseph Wood (2011-2014).
Abarasi worked as an assistant lecturer at the Department of Chemical Engineering, University of Port Harcourt (2008-2012). After his PhD, he accepted a postdoctoral fellowship on the application of bio nano particles for in situ upgrading of heavy oil in the THAI-CAPRI process at the University of Birmingham, UK (4/2014 – 9/2015). He has published over 38 peer-reviewed papers.
The research project involved four partners: School of Biosciences UoB, University of Nottingham, University of Manchester, and Touchstone Exploration Inc, Canada. He is currently a research fellow on Electromagnetically-assisted Catalytic-upgrading of Heavy Oil (ECHO), collaborating with University of Nottingham and PetroChina, and he also coordinates research students

Joe Wood

Joe Wood qualified with a BEng degree in Chemical Engineering with Environmental Protection from Loughborough University in 1995. He worked at Albright and Wilson in Whitehaven from 1995-97 as a Graduate Chemical Engineer. He then studied for a PhD at the University of Cambridge, with thesis topic Transport and Reaction in Porous Catalysts under the supervision of Professor Lynn Gladden, which was awarded in 2001. Since 2001 he has worked at the University of Birmingham as Lecturer (2001-2008), Senior Lecturer (2008-2010), Reader (2010-2012) and Professor (2012-Present).
Professor Wood held a Junior Research Fellowship at Hughes Hall Cambridge from 1998-2000 and an Exxon Mobil Teaching Fellowship from 2004-2007.
Professor Wood's research focuses on the application of catalysis and reactor engineering to solve problems of energy supply, environmental concerns and to deliver chemical products in a more sustainable way.
He teaches on Chemical Engineering programmes in the School, is Examinations Officer and IChemE Liaison Officer.

Yi Wang

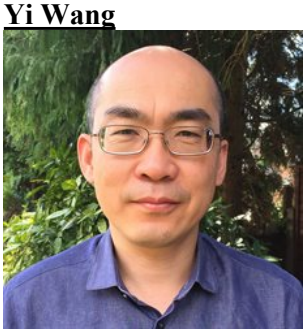

Yi Wang received his BSc and MSc in Physics from the University of Science and Technology Beijing, China, in 1998 and 2001 respectively, and his PhD degree in Electronic and Electrical Engineering from University of Birmingham, UK, in 2005. His career began as a research fellow at University of Birmingham from 2004, working on high-frequency devices for communications and radars using advanced materials (e.g. superconductors, ferroelectric, SU-8 photoresists), novel structures (e.g. left-handed metamaterials) and micro-fabrication techniques (MEMS and micromachining). In 2011, he became a Senior Lecturer and then Reader at the University of Greenwich. In 2018, Yi joined Birmingham as a Senior Lecturer.
Yi Wang has published over 140 peer-reviewed papers. He has a breadth of knowledge and expertise in microwave circuit design, micro-fabrications, microwave and antenna measurements, and electronic materials. Dr Wang has been appointed as a visiting Professor of Shanghai Institute of Ceramics (microwave materials and devices), Chinese Academy of Science between 2017 and 2020. His current research interests include millimeter-wave and terahertz devices for metrology, communications and sensors, micromachining, 3D printing, microwave circuits based on multiport filtering networks, and filter-antenna integration.

M. J. Lancaster

Michael J. Lancaster was born in England in 1958. He was educated at Bath University, UK, where he graduated with a degree in Physics in 1980. His career continued at Bath, where he was awarded a PhD in 1984 for research into non-linear underwater acoustics.

After leaving Bath University he joined the surface acoustic wave (SAW) group at the Department of Engineering Science at Oxford University as a Research Fellow. The research was in the design of new, novel SAW devices, including filters and filter banks. In 1987 he became a Lecturer at The University of Birmingham in the Department of Electronic and Electrical Engineering, lecturing in electromagnetic theory and microwave engineering. Shortly after he joined the department he began the study of the science and applications of high temperature superconductors, working mainly at microwave frequencies. He was promoted to head the Emerging Device Technology Research Centre in 2000 and head of the department of Electronic, Electrical and Systems Engineering in 2003. His present personal research interests include microwave filters and antennas, as well as the high frequency properties and applications of a number of novel and diverse materials.

Professor Lancaster is Fellow of the IET and UK Institute of Physics. He is a Chartered Engineer and Chartered Physicist. In addition he is a fellow of the UK Higher Education Academy. He has served on the MTT IMS technical committee. Professor Lancaster has published two books and over 220 papers in refereed journals.